Non-hydrothermal Synthesis of Cylindrical Mesoporous Materials: The Influence of the *Surfactant/Silica* molar ratio

Deicy Barrera, Jhonny Villarroel Rocha, Luis Marenco, Karim Sapag*

Laboratorio de Sólidos Porosos. Instituto de Física Aplicada. CONICET. Universidad Nacional de San Luis. Chacabuco 917. 5700. San Luis. Argentina

* Corresponding author:

e-mail: sapag@unsl.edu.ar

Phone: +54 2652 423789 int 125

Fax: +54 2652 436151

Abstract

Ordered mesoporous materials type MCM-41 and SBA-15 were synthesized under non-hydrothermal conditions using different molar ratio of surfactant/silica, from 0.07 to 0.27 for MCM-41 and from 0.009 to 0.021 for SBA-15. N_2 adsorption–desorption isotherms at 77 K were used to evaluate the specific surface areas obtaining values up to 1450 and 1100 m^2/g for MCM-41 and SBA-15, respectively. Scanning electron microscopy was carried out to study the morphology of the materials. The size of primary mesopores and the pore thicknesses were assessed by a geometrical method using X-ray diffraction and N_2 adsorption data. Results of the pore size were compared with those obtained by a recently reported method (VBS-method) and the Non-Local Density Functional Theory model, both proposed to evaluate the pore size distribution of these materials. It was found that under the synthesis conditions the surfactant/silica molar ratio has an important consequence in the final characteristics of these materials.

Keywords

Ordered mesoporous silica, Non-hydrothermal synthesis, Surfactant/silica molar ratio, Pore wall thickness, Primary mesopore size.

1 Introduction

Ordered mesoporous materials (OMM) have played a major role in modern technology because of their chemical, biochemical and environmental applications as catalyst supports and adsorbents, particularly in reactions involving large molecules (Xiao and Han 2004; Taguchi and Schüth 2005; Szegedi *et al.* 2009). Nevertheless, mesoporous silica materials have attracted attention in the science materials due to their morphological and textural properties, such as high specific surface area, large pore volumes, narrow pore size distribution, wide pore dimensions and regular pore structure (Zhao *et al.* 1996; Galarneau *et al.* 2001). As a result, silica structures and pore sizes allow the access of large molecules and enhance catalytic activity and adsorptive capacity compared to microporous materials (Beck *et al.* 1992).

MCM-41 (Zhao *et al.* 1996) and SBA-15 (Ravikovitch and Neimark 2001) have been the mesoporous materials most widely studied, not only due to their high structural regularity but also because of diverse pore sizes and wall thicknesses can be *designed* through the appropriate synthesis conditions. The pore sizes of the MCM-41 and SBA-15 materials fall between 20 and 100 Å, and 20 and 300 Å, respectively (Thommes 2004). Structurally, the MCM-41 and SBA-15 materials are ordered in hexagonal arrangements of cylindrical channels (Thommes *et al.* 2002), where SBA-15 exhibits intrawall micropores connecting the primary mesopores, which are the internal part of the cylindrical channels (Galarneau *et al.* 2003).

Thermal stability of the mesoporous materials is strongly related to the silica wall thickness (Galarneau *et al.* 2001; Cassiers *et al.* 2002). Thus, the design of materials with controllable wall thickness could be an interesting alternative in the catalysis area, where high thermal conditions are required.

MCM-41 and SBA-15 materials have been prepared using a variety of procedures under hydrothermal, microwave or room (non-hydrothermal) conditions (Selvam *et al.* 2001), being the former one the most used. These procedures are commonly carried out in presence of a surfactant, usually alkyl-trimethyl-ammonium and non-ionic tri-block copolymer for MCM-41 and SBA-15, respectively (Khushalani *et al.* 1995; Sayari *et al.* 1997; Zhao *et al.* 1998; Zhang *et al.* 2005). Several studies under hydrothermal conditions have shown that the synthesis of this type of materials depends on various factors influencing on their final properties. These factors are: silica source (Selvam *et al.* 2001; Fulvio *et al.* 2005), surfactant chain length (Beck *et al.* 1992; Kruk *et al.* 2003), surfactant/silica ratio (Vartuli *et al.* 1994; Miyazawa *et al.* 1998), solvent properties (Anderson *et al.* 1998), swelling agent (Kim and Yang 2000), inorganic salts addition (Zhang *et al.* 2005; Ryoo and Jun 1997), aging time (Zhao *et al.* 1998; Nan *et al.* 2009), method of template removal (Raman *et al.* 1996) and temperature of synthesis (Galarneau *et al.* 2003; Cassiers *et al.* 2002). The control of these factors results in materials of high quality and defined structure. But, the variation of the surfactant/silica ratio has been one of the most interesting factors allowing the *design* of different pore wall thickness of highly ordered mesoporous silica (Yu *et al.* 2001). However, extensive studies have not been performed on the synthesis of OMM under *non-hydrothermal* conditions. As regards of the surfactant/silica molar ratio in the MCM-41 and SBA-

15 synthesis, the typical values previously reported are 0.12 (Vallet-Regi *et al.* 2001; Baute *et al.* 2005) and 0.017 (Zhao *et al.* 1998; Kruk *et al.* 2000), respectively.

In this work, a synthesis of type materials MCM-41 and SBA-15 under non-hydrothermal conditions were carried out. Tetraethyl orthosilicate (TEOS) was used as silica source for both materials and cetyltrimethylammonium bromide (CTAB) and Pluronic P123 were used as surfactants for MCM-41 and SBA-15 synthesis, respectively. Four samples of each type of mesoporous material were prepared varying the surfactant/silica molar ratio, controlling, optimizing and setting the other factors in the synthesis. The OMM were characterized using X-ray diffraction (XRD), scanning electron microscopy (SEM) and nitrogen sorption measurements with the aim of evaluating their structural, textural and morphological properties and finding a relation among them and the variation in the surfactant/silica molar ratio.

2 Experimental

2.1 Materials

Two families of ordered mesoporous materials, MCM-41 and SBA-15, were synthesized by the sol-gel method. Four variations in surfactant/silica molar ratio were applied to each one.

***MCM-41 samples*:**

These materials were synthesized at room temperature and without hydrothermal treatment according to a modification of Grün et al. procedure (Grün *et al.* 1999). CTAB ($C_{16}H_{33}N(CH_3)_3Br$ – Merck) was used as surfactant, TEOS ($SiC_8H_{20}O_4$ - Merck) as silica source, NaOH as catalyst and water as solvent. Molar ratios used for the preparation of the MCM-41 samples were: ***x***CTAB:***1***TEOS:***0.6***NaOH:***100***H_2O where ***x*** corresponds to the molar ratio of CTAB/TEOS. The CTAB was suspended in deionized water and then mixed with an aqueous solution of 1 M NaOH in vigorous stirring until a transparent solution was obtained. Subsequently, TEOS was added drop-wise to form an emulsion that was stirred for 24 h. The obtained solids were separated by filtration, washed with abundant deionized water up to a conductivity value smaller than 10 μS/cm (conductivity of the deionized water), dried at 60 °C for 12 h and calcined at 550 °C for 6 h at a heating rate of 1 °C/min. The ***x*** ratio was varied, obtaining four samples (M1, M2, M3 and M4) described in Table 1.

***SBA-15 samples*:**

These materials were obtained based on a modification to the synthesis process described by Esparza *et al.* (2005). The used reagents were: the surfactant Pluronic P123 triblock copolymer, P123 (EO_{20}-PO_{70}-EO_{20} – Aldrich), TEOS and HCl. The molar ratios used for the preparation of the SBA-15 were: ***y***P123:***1***TEOS:***6***HCl:***140***H_2O, where ***y*** corresponds to the molar ratio of P123/TEOS. P123 was dissolved in an aqueous solution of 2 M HCl (pH=1) and kept under stirring at 40 °C for 2 h. The required quantity of TEOS was added drop-wise and kept under vigorous stirring for 4 h at the same temperature. Afterwards, the reaction mixture was aged for 20 h at 40 °C without stirring. Subsequently, the temperature was raised to 80 °C and maintained at this value for 48 h. The solids were filtrated, washed with abundant deionized water until reaching a conductivity value smaller than 10 μS/cm, dried at 60 °C for 12 h and calcined at 550 °C for 6 h at 1 °C/min. The ***y*** was varied obtaining four samples (S1, S2, S3 and S4) described in Table 1.

2.2 Characterization

Measurements of N_2 (99.999 %) adsorption-desorption at 77 K were carried out using a volumetric adsorption equipment (AUTOSORB-1MP, Quantachrome Instruments). Samples were previously degassed at 150 °C for 12 h, up to residual pressure was minor than 0.5 Pa. XRD measurements were performed on a Rigaku D-MAX IIIC diffractometer using nickel-filtered Cu Kα radiation from 1 to 10° of 2θ. SEM images were obtained on a LEO 1450VP microscope.

2.3 Calculations

The Brunauer, Emmet and Teller (BET) method (Brunauer *et al.* 1938) was used to estimate the specific surface area (S_{BET}) of the samples, using the nitrogen adsorption data in the range of relative pressures from 0.05 to 0.12 and 0.05 to 0.2 for MCM-41 and SBA-15, respectively. The total pore volume (V_{TP}) was obtained by the Gurvich's rule (Rouquerol *et al.* 1999) from the isotherms at a relative pressure of 0.98. To calculate the micropore ($V_{\mu P}$) and primary mesopore (V_{PMP}) volumes, using the LiChrospher Si-1000 macroporous silica gel as the reference adsorbent (Jaroniec *et al.* 1999), the α_s-plot method was used (Sayari *et al.* 1997; Gregg and Sing 1984). The volume of secondary mesopores (V_{SMP}) was obtained from the difference between V_{TP} and the sum of $V_{\mu P}$ and V_{PMP}.

The pore size distribution (PSD) was obtained using the macroscopic method on the desorption branch described by Villarroel-Rocha, Barrera and Sapag (VBS method) (Villarroel-Rocha *et al.* 2011). This is a method recently proposed to improve the study of PSD in OMM, based on the BJH algorithm, with a correction term f_c obtained by adjusting the experimental isotherms with a set of simulated isotherms. The Non-Local Density Functional Theory (NLDFT) method also was used, comparing the obtained results with VBS method. The kernel used in the NLDFT method on the desorption branch was: "N_2 at 77 K on silica, NLDFT equilibrium model" (Ravikovitch *et al.* 1997) for materials with cylindrical pores, in the range of pore sizes from 3.5 to 1000 Å.

On the other hand, pore sizes were also calculated using a method based in a simple geometrical relation between the interplanar spacing, the pore volumes and the pore diameter for an infinite array of cylindrical pores with hexagonal structure (Figure 1). The pore size ($w_{p\text{-}XRD}$) for each sample was obtained from the micropores volume ($V_{\mu P}$), the primary mesoporous volume (V_{PMP}) and the interplanar spacing d_{100}, by means of the Equation 1 (Sayari *et al.* 1997; Kruk *et al.* 1999).

$$w_{p-XRD} = \left(\frac{8}{\sqrt{3}\cdot\pi}\right)^{1/2} \cdot d_{100} \cdot \left(\frac{V_{PMP}}{1/\rho + V_{PMP} + V_{\mu P}}\right)^{1/2} \qquad \textbf{(1)}$$

where ρ is the pore wall density, which is 2.2 g/cm^3 for the pore walls of amorphous silica (Marler *et al.* 1996). In addition, the distance between the pore centers (a) and the pore wall thickness (e) for MCM-41 and SBA-15 were obtained with the same geometrical method by means of the Equations 2 and 3.

$$a = \frac{2}{\sqrt{3}} \cdot d_{100} \qquad \textbf{(2)}$$

$$e = a - w_p \qquad \textbf{(3)}$$

X-ray diffractions were not carried out to small angle (below 1° in 2Θ) and the peak corresponding to the reflection *100* of the mesoporous materials SBA-15 could not be observed (See Figure 2). However, with the knowledge that this kind of materials present a hexagonal structure P6mm (Selvam *et al.* 2001; Zhao *et al.* 1998), the reflection *200* could be used to estimate the interplanar space d_{100}, being $d_{100} = 2 \cdot d_{200}$, which is schematically shown in Figure 1.

3 Results and discussions

X-ray diffraction patterns of MCM-41 and SBA-15 samples are displayed in Figure 2. Figure 2a shows the MCM-41 difractograms exhibiting the characteristic (100) diffraction peak. In addition, it is possible to observe a small signal associated to the overlapped (110) and (200) reflections, typical for hexagonal cell array. The apparition of the reflections (110) and (200) suggests the presence of channels in hexagonally arrangement but, the weak intensity of these interplanar distances might indicates that this array is not very regular. But to ensure this would have to make more accurate measurements, e.g. by using a synchrotron line. The difractograms in the Figure 2a indicate that when the CTAB/TEOS molar ratio is increased the position of the peak (100) shifts gradually to higher 2θ angles (see Table 3), suggesting a decreasing of the mesopore size or of the pore wall thickness or both. Figure 2b shows the patterns of the SBA-15 samples, where the (100) reflection cannot be seen in this analysis, as it was before mentioned. Nevertheless, it is possible to observe other peaks, (110) and (200) reflections, typical of SBA-15 type materials. These patterns indicate that when the P123/TEOS molar ratio increases, the positions of the (110) and (200) peaks shifts gradually to higher 2θ angles. As aforementioned, the d_{100} peaks are obtained from the d_{200} peaks. Then, an increase in P123/TEOS molar ratio suggests a decrease of the mesopore sizes or/and of the pore wall thickness, for the SBA-15 samples.

Figures 3 and 4 show the micrographs of the set of MCM-41 and SBA-15 synthesized samples, respectively. In Figure 3 can be seen an agglomerate of particles and the raise in the particle sizes when the CTAB/TEOS molar ratio increases. In the case of the lowest molar ratio (Figure 3a), small particles that resemble spheres and are linked together are observed. When the amount of surfactant is increased the individual particles shape is lost (Figures 3b, 3c and 3d).

Figure 4 shows a rod-like morphology in all samples. Similar morphologies of SBA-15 materials were reported (Liu *et al.* 2004; Shen *et al.* 2006). In Figure 4a, is observed that all particles are ordered in the same direction and when the P123/TEOS molar ratio increases, the particles reach more defined shapes and uniform sizes, but losing the unique direction. The last sample, S4 (Figure 4d), shows a morphology with particles stacked among them and the loss of degree of order. Figure 4c shows the most uniform particle sizes with dimensions ca. 0.45 μm and ca. 0.55 μm in width and length, respectively.

Figure 5 illustrates the experimental N_2 adsorption-desorption isotherms at 77 K for the materials under study. To clarify the view of the isotherm forms, some of them were translated in vertical direction (indicated in the corresponding Figure captions). Both kinds of materials, MCM-41 and SBA-15, exhibit type IV isotherms according to the IUPAC classification (Sing *et al.* 1985), which are typical for mesoporous materials (Kruk and Jaroniec 2001).

The isotherms for the MCM-41 materials are shown in Figure 5a. As could be observed, all samples are reversible approximately up to 0.4 in P/P_0 and at higher relative pressures show a small hysteresis loop of the type H4, typical of materials with inter-particle pores, corresponding to secondary mesopores (Sing *et al.* 1985). From the isotherms can be observed: a) high adsorption at low relative pressures due to a strong adsorbate-adsorbent interaction; b) a step that corresponds to the filling of primary mesopores at a P/P_0 interval between 0.1 and 0.35, where a pronounced inflexion qualitatively indicates a defined primary mesopore size; c) a slight increase of the amount adsorbed when P/P_0 is higher than 0.4 indicating the presence of a little amount of larger pores than primary mesopores and d) the hysteresis loops close at relative pressures near to 0.42, showing the presence of interconnected pores. In addition, when the CTAB/TEOS molar ratio increases, the isotherms show: *i)* the loss gradually of their hysteresis loops, indicating a same mechanism in filling and emptying secondary mesopores (with N_2), and *ii)* the interval in relative pressures of the capillary condensation stage of the primary mesoporous not shifts, indicating that the pore size might be the same in all samples.

The isotherms of the SBA-15 materials (Figure 5b) show hysteresis loops of the type H1, typical of these mesoporous materials. However, the S1 sample shows a hybrid loop of hysteresis between the types H1 and H3 (Sing *et al.* 1985). The isotherms of the SBA-15 samples are reversible up to a P/P_0 of 0.6, except for the S1 sample that is until a P/P_0 of 0.45. For the Figure 5b can be noted: a) the adsorption at very low pressures ($P/P_0 < 0.05$) is due to the filling of the micropores (or strong interaction adsorbate-adsorbent) and the adsorption at high pressures ($0.05 < P/P_0 < 0.7$) to monolayer-multilayer adsorption of N_2 on the walls of the mesopores; b) the capillary condensation (adsorption branch) takes place on the primary mesopores at relative pressures higher than 0.7 up to approximately 0.8 where the secondary mesoporous begin filling; the pronounced inflexion indicates a definite primary mesopore size; c) the hysteresis loops in the desorption branches show a sharp fall at a P/P_0 near to 0.6, except for the S1 sample which present an extended hysteresis closing finally at a P/P_0 of 0.45, due to the presence of blocked mesopores (Kruk and Jaroniec 2001); d) the adsorption and desorption branches in the hysteresis loops are parallels, typical of materials with cylindrical geometries with uniform pore sizes. Additionally, when the P123/TEOS molar ratio decreases, can be distinguished: *i)* the generation of constrictions in the primary mesopores (S1 sample), as was reported (Van Der Voort *et al.* 2002; Grosman and Ortega 2005); *ii)* a decrease in the slope of the plateau of the isotherms ($P/P_0 > 0.8$), indicating a decrease of external surface area, relating with cylinders more aligned, as was seen in the SEM analysis and *iii)* the position of the steps of the capillary condensation and capillary evaporation of the primary mesoporous does not change significantly, indicating a similar primary mesopore size in the samples.

The α_s-plots of the M1 and S1 samples are shown in Figure 6. It can see that there are well-defined regions: *i)* a not linear region at low α_s values (low P/P_0) due to adsorption in micropores; this region is absent in the M1 sample; *ii)* a linear region due to the monolayer-multilayer adsorption in mesopores, in this region the micropores are filled; *iii)* a region where the adsorbed amount increases quickly due to capillary condensation in the primary mesopores; *iv)* a last region due to the adsorption in secondary mesopores and on the external surface, where in the first part (linear region) the mesopores are filled. The other samples showed a similar behavior.

In general, the volumes of micropores were evaluated using the range of α_s values from 0.15 to 0.6 and 0.6 to 1.0 for the MCM-41 and SBA-15, respectively. The results show the absence of micropores in the MCM-41 samples. The volumes of primary mesopores and the external surface areas were determined using the range of α_s values from 1.1 to 1.5 and 1.8 to 2.4 for the MCM-41 and SBA-15 samples, respectively. In all cases, a good linear correlation coefficient was obtained ($R^2 > 0.995$).

The data of the textural properties of the materials determined from the N_2 adsorption isotherms at 77 K as shown in Table 2. It can be noted that when the surfactant/TEOS increases: a) the micropores volume ($V_{\mu P}$) in SBA-15 samples decreases, while, the MCM-41 samples not present microporosity; b) for both materials, the primary mesopores volumes (V_{PMP}) increases and therefore the specific surface area (S_{BET}), with values from 1075 to 1450 m^2/g and 925 to 1110 m^2/g for MCM-41 and SBA-15, respectively. Specific surface areas reported for MCM-41 (Sayari *et al.* 1997; Kruk *et al.* 2000; Kruk *et al.* 1997; Lelong *et al.* 2008) and SBA-15 materials (Zhao *et al.* 1998; Kruk *et al.* 2003; Van Der Voort *et al.* 2002; Kruk *et al.* 2000) synthesized under hydrothermal conditions are lower than the obtained in this work and c) the external surface (S_{ext}) as well as the secondary mesoporous volume (V_{SMP}) decreases in the case of MCM-41 materials, in contrast to SBA-15 materials where these properties increase.

Figure 7 shows the pore size distribution (PSD) of each material evaluated by the VBS macroscopic method. In Figure 7a, is shown a significant peak for all the MCM-41 samples, associated to primary mesopores and a small additional peak with disappear as CTAB/TEOS molar ratio increases. Could be noted that the primary mesopore size not vary considerably, with values between 3.4 to 3.6 nm. The second peak is related to the interconnected secondary mesoporous. In Figure 7b, can be observed a defined pore size for each SBA-15 sample related to the primary mesopore size, with values between 7.8 and 8.2 nm. The PSD of S1 sample presents an additional peak corresponding to the blocked primary mesoporous.

In the Table 3 are shown the data obtained by using equations 1, 2 and 3 and the size of primary mesopores calculated by using the VBS method and NLDFT model. The pore sizes obtained by the VBS method were in agreement with those found by the NLDFT model and both are different with the data obtained from Equation 1 ($\boldsymbol{w_{p\text{-}XRD}}$). This difference may be attributed to several causes in the application of the geometrical method, e.g. *i)* a perfect hexagonal arrangement for the primary mesoporous is assumed *ii)* a constant density value is used in all of type of materials. Nevertheless, regards to the study of variation in the surfactant/TEOS molar ratio, the three evaluation ways of the pore size used herein are consistent.

From the data showed in the Table 3 is important to remark that the increase of surfactant/TEOS molar ratios for both types of materials produces a decrease in the thickness of the pore walls but not a change in the pore sizes. This behavior could be according with the fact that to the pore size is defined by the micelle size, which varies depending on carbon chain length of surfactant. In the synthesis, the surfactant chain length was the same for each material type (CTAB and P123 for MCM-41 and SBA-15, respectively), only the quantity of surfactant was increased without a variation in the incorporated silica. The same quantity of the silica should be distributed in an increased quantity of micelles, generating an increased quantity of cylinders with a decreasing wall thickness. In Figure 8 is presented a schematic representation of these results showing the increase of the number of cylinder with the same pore size and a decrease in the wall thickness when the surfactant/TEOS molar ratio increase.

4 Conclusions

MCM-41 and SBA-15 ordered mesoporous materials of high quality were obtained with different surfactant/silica molar ratios (S/S) under non-hydrotermal conditions. The structural characteristics of all the samples carried out by XRD analysis revealed that an increase in the S/S produces a decreasing in their interplanar distance, associated to a reduction in the size of the cylinders in transversal direction.

Regarding to the SEM analysis, the MCM-41 sample with the lowest S/S presents small spherical particles linked together. An increase in their sizes and the loss of the initial geometry was observed when the S/S was increased. The SBA-15 samples show a rod-like geometry for all the set. The sample with the lowest S/S displayed a directional order that is lost when the S/S is increased. These materials, MCM-41 and SBA-15, show a disorder in their morphology as the S/S is increased.

A deeper analysis of the textural characteristics of these samples was accomplished by adsorption-desorption of nitrogen a 77 K, obtaining important conclusions:

The specific surface areas obtained for the samples MCM-41 and SBA-15 under non-hydrothermal synthesis were higher than reported in similar materials synthesized by other methods.

MCM-41 samples, as known, do not show the presence of micropores and the micropores volume of SBA-15 samples decreases when the S/S is increased.

MCM-41 samples with the lowest S/S showed a small hysteresis loop which is lost when the S/S was increased. SBA-15 sample with the lowest S/S presented blocked mesopores.

The use of the VBS method for evaluating the PSD of the samples provided a specific analysis of their pore sizes. The data obtained by using this method were compared to those of the NLDFT method, certifying the use of the VBS method for mesoporous materials.

Finally, an increase in the S/S produced samples with a higher quantity of cylindrical pores and similar primary mesopore size but, with less silica wall thickness.

Acknowledgments

This work was financially supported by FONCYT, UNSL and CONICET (Argentina).

References

Anderson, M.T., Martin, J.E., Odinek, J.G. and Newcomer, P.P. (1998) *Chem. Mater.* **10,** 311.

Baute, D., Zimmermann, H., Kababya, S., Vega, S. and Goldfarb, D. (2005) *Chem. Mater.* **17,** 3723.

Beck, J.S., Vartuli, J.C., Roth, W.J., Leonowicz, M.E., Kresge, C.T., Schmitt, K.D., Chu, C.T.W., Olson, D.H., Sheppard, E.W., McCullen, S.B., Higgins, J.B. and Schlenker, J.L. (1992) *J. Am. Chem. Soc.* **114,** 10834.

Brunauer, S., Emmett, P.H, and Teller, E. (1938) *J. Am. Chem. Soc.* **60,** 309.

Cassiers, K., Linssen, T., Mathieu, M., Benjelloun, M., Schrijnemakers, K., Van Der Voort, P., Cool, P. and Vansant, E.F. (2002) *Chem. Mater.* **14,** 2317.

Esparza, J.M., Ojeda, M.L., Campero, A., Hernández, G., Felipe, C., Asomoza, M., Cordero, S., Kornhauser, I. and Rojas, F. (2005) *J. Mol. Catal. A* **228,** 97.

Fulvio, P.F., Pikus, S. and Jaroniec, M. (2005) *J. Colloid Interf. Sci.* **287,** 717.

Galarneau, A., Cambon, H., Di Renzo, F., Ryoo, R., Choib, M. and Fajula, F. (2003) *New J. Chem.* **27,** 73.

Galarneau, A., Desplantier-Giscard, D., Di Renzo, F. and Fajula, F. (2001) *Catal. Today* **68,** 191.

Gregg, S.J. and Sing, K.S.W. (1982) *Adsorption, surface area and porosity*, 2nd Edn, Academic Press, New York.

Grosman, A. and Ortega, C. (2005) *Langmuir* **21,** 10515.

Grün, M., Unger, K.K., Matsumoto, A. and Tsutsumi, K. (1999) *Micropor. Mesopor. Mat.* **27,** 207.

Jaroniec, M., Kruck, M. and Olivier, J. (1999) *Langmuir* **15,** 5410.

Khushalani, D., Kuperman, A., Ozin, G.A., Tanaka, K., Coombs, N., Olken, M.M. and Garcés, J. (1995) *Adv. Mater.* **7,** 842.

Kim, W.-J. and Yang, S.-M. (2000) *Chem. Mater.* **12,** 3227.

Kruk, M. and Jaroniec, M. (2001) *Chem. Mater.* **13,** 3169.

Kruk, M., Jaroniec, M. and Sayari, A. (1997) *Langmuir* **13,** 6267.

Kruk, M., Jaroniec, M. and Sayari, A. (1999) *Chem. Mater.* **11,** 492.

Kruk, M., Jaroniec, M., Hoon Joo, S. and Ryoo, R. (2003) *J. Phys. Chem. B* **107,** 2205.

Kruk, M., Jaroniec, M., Hyun Ko, C. and Ryoo, R. (2000) *Chem. Mater.* **12,** 1961.

Kruk, M., Jaroniec, M., Sakamoto, Y., Terasaki, O., Ryoo, R. and Hyun Ko, C. (2000) *J. Phys. Chem. B* **104,** 292.

Lelong, G., Bhattacharyya, S., Kline, S., Cacciaguerra, T., Gonzalez, M.A. and Saboungi, M-L. (2008) *J. Phys. Chem. C* **112,** 10674.

Liu, Y.-M., Cao, Y., Yi, N., Feng, W.-L., Dai, W.-L., Yan, S.-R., He, H.-Y. and Fan, K.-N. (2004) *J. Catal.* **224,** 417.

Marler, B., Oberhagemann, U., Vortmann, S., and Gies, H. (1996) *Microporous Mater.* **6,** 375.

Miyazawa, K. and Inagaki, S. (2000) *Chem. Commun.* **21,** 2121.

Nan, Z., Wang, M. and Yan, B. (2009) *J. Chem. Eng. Data* **54,** 83.

Raman, N.K., Anderson, M.T. and Brinker, C.J. (1996) *Chem. Mater.* **8,** 1682.

Ravikovitch, P.I, Wei, D., Chueh, W.T., Haller, G.L. and Neimark, A.V. (1997) *J. Phys. Chem. B* **101,** 3671.

Ravikovitch, P.I. and Neimark, A.V. (2001) *J. Phys. Chem. B* **105,** 6817.

Rouquerol, F., Rouquerol, J. and Sing, K. (1999) *Adsorption by powders & porous solids*, Academic Press, San Diego.

Ryoo, R. and Jun, S. (1997) *J. Phys. Chem. B* **101,** 317.

Sayari, A., Liu, P., Kruk, M. and Jaroniec, M. (1997) *Chem. Mater.* **9,** 2499.

Selvam, P., Bhatia, S.K. and Sonwane, C.G. (2001) *Ind. Eng. Chem. Res.* **40,** 3237.

Shen, S., Chen, F., Chow, P.S., Phanapavudhikul, P., Zhu, K. and Tan, R.B.H. (2006) *Micropor. Mesopor. Mat.* **92,** 300.

Sing, K.S.W., Everett, D.H., Haul, R.A.W., Moscou, L., Pierotti, R.A., Rouquerol, J. and Siemieniewska, T. (1985) *Pure Appl. Chem.* **57,** 603.

Szegedi, A., Popova, M. and Minchev, C. (2009) *J. Mater. Sci.* **44,** 6710.

Taguchi, A. and Schüth, F. (2005) *Micropor. Mesopor. Mat.* **77,** 1.

Thommes, M. (2004) Physical adsorption characterization of ordered and amorphous mesoporous materials, in *Nanoporous Materials: Science and Engineering – Series on Chemical Engineering*, Vol. 4, Lu, G.Q. and Zhao, X.S., Eds, Imperial College Press, London, p. 317.

Thommes, M., Köhn, R. and Fröba, M. (2002) *Appl. Surf. Sci.* **196,** 239.

Vallet-Regi, M., Rámila, A., del Real, R.P. and Pérez-Pariente, J. (2001) *Chem. Mater.* **13,** 308.

Van Der Voort, P., Ravikovitch, P.I., De Jong, K.P., Benjelloun, M., Van Bavel, E., Janssen, A.H., Neimark, A.V., Weckhuysen, B.M. and Vansant, E.F. (2002) *J. Phys. Chem. B* **106,** 5873.

Vartuli, J.C., Schmitt, K.D., Kresge, C.T., Roth, W.J., Leonowicz, M.E., McCullen, S.B., Hellring, S.D., Beck, J.S., Schlenker, J.L., Olson, D.H. and Sheppardt, E.W. (1994) *Chem. Mater.* **6,** 2317.

Villarroel Rocha, J., Barrera, D. and Sapag, K. (2011) *Top. Catal.* **54,** 121.

Xiao, F.S. and Han, Y. (2004) Acidity-enhanced nanoporous catalytic materials, in *Nanoporous Materials: Science and Engineering – Series on Chemical Engineering*, Vol. 4, Lu, G.Q. and Zhao, X.S., Eds, Imperial College Press, London, p. 519.

Yu, J., Shi, J.-L., Wang, L.-Z., Ruan, M.-L. and Yan, D.-S. (2001) *Mater. Lett.* **48,** 112.

Zhang, F., Yan, Y., Yang, H., Meng, Y., Yu, C., Tu, B. and Zhao, D. (2005) *J. Phys. Chem. B* **109,** 8723.

Zhao, D., Feng, J., Huo, Q., Melosh, N., Fredrickson, G.H., Chmelka, B.F. and Stucky, G.D. (1998) *Science* **279,** 548.

Zhao, D., Huo, Q., Feng, J., Chmelka, B. and Stucky, G. (1998) *J. Am. Chem. Soc.* **120,** 6024.

Zhao, X.S., Lu, G.Q. and Millar, G.J. (1996) *Ind. Eng. Chem. Res.* **35,** 2075.

Figure captions

Figure 1. Scheme of the geometrical structure of cylindrical pores in OMM

Figure 2. X-ray diffraction patterns of a) MCM-41 and b) SBA-15 materials

Figure 3. SEM images of MCM-41 materials for the samples: a) M1, b) M2, c) M3 and d) M4

Figure 4. SEM images of SBA-15 materials for the samples: a) S1, b) S2, c) S3 and d) S4

Figure 5. N_2 adsorption-desorption experimental isotherms at 77 K for: a) MCM-41 and b) SBA-15 materials. The adsorbed amounts for M3, M4, S2, S3 and S4 were incremented by 50, 75, 200, 400 and 600 cm^3/g, respectively. The isotherms are plotted from down to up with the increase of surfactant/silica molar ratio

Figure 6. α_s-plot for MCM-41 and SBA-15 materials: a) M1 and b) S1 sample

Figure 7. Pore size distribution for MCM-41 and SBA-15 materials using VBS method. The PSD are plotted from down to up with the increase of surfactant/silica molar ratio

Figure 8. Schematic representation of the effect of the surfactant/TEOS molar ratio in the final characteristics of MCM-41 and SBA-15 materials

Table captions

Table 1. Surfactant/TEOS molar ratios in the synthesis of the MCM-41 and SBA-15 samples

Table 2. Textural properties of the MCM-41 and SBA-15 samples

Table 3. Size and thickness of primary mesopores of the MCM-41 and SBA-15 samples by XRD and N_2 adsorption-desorption analysis

Figure 1

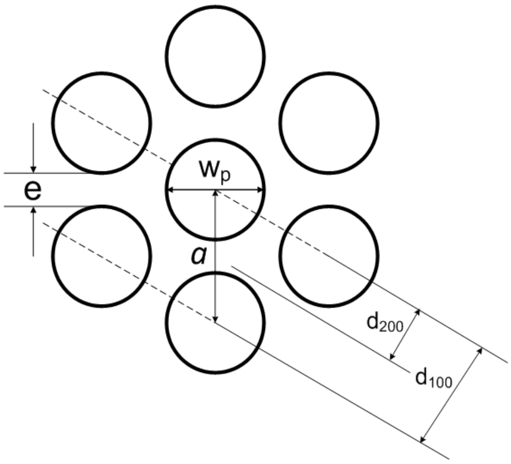

Figure 2

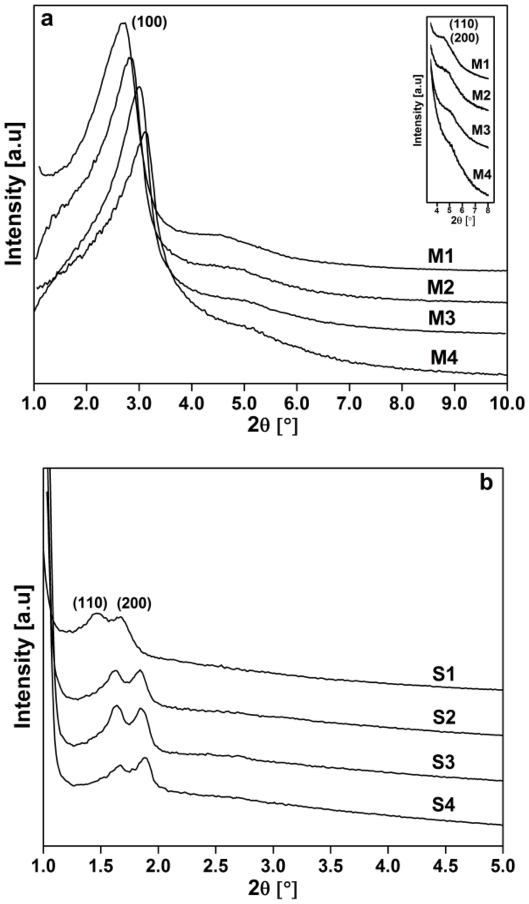
a
(100)
Intensity [a.u]
M1
M2
M3
M4
1.0
2.0
3.0
4.0
5.0
6.0
7.0
8.0
9.0
10.0
2θ [°]
(110)
(200)
Intensity [a.u]
M1
M2
M3
M4
4
5
6
7
8
2θ [°]
b
(110)
(200)
Intensity [a.u]
S1
S2
S3
S4
1.0
1.5
2.0
2.5
3.0
3.5
4.0
4.5
5.0
2θ [°]

Figure 3

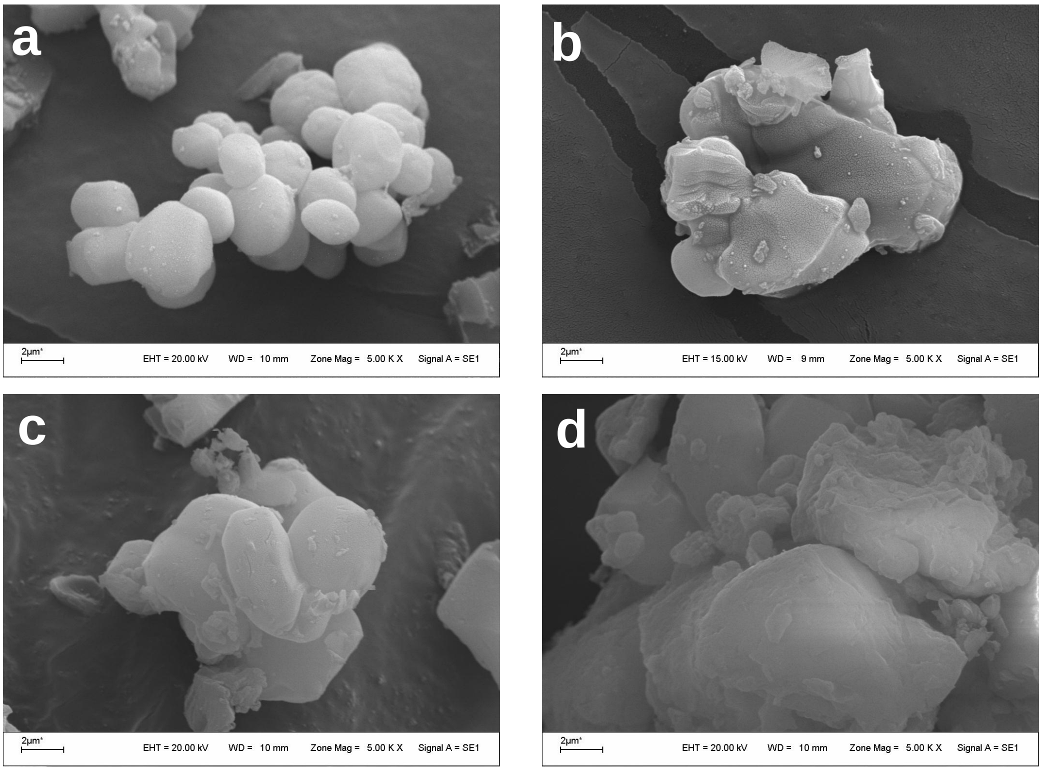
a
2µm*
EHT = 20.00 kV
WD = 10 mm
Zone Mag = 5.00 K X
Signal A = SE1
b
2µm*
EHT = 15.00 kV
WD = 9 mm
Zone Mag = 5.00 K X
Signal A = SE1
c
2µm*
EHT = 20.00 kV
WD = 10 mm
Zone Mag = 5.00 K X
Signal A = SE1
d
2µm*
EHT = 20.00 kV
WD = 10 mm
Zone Mag = 5.00 K X
Signal A = SE1

Figure 4

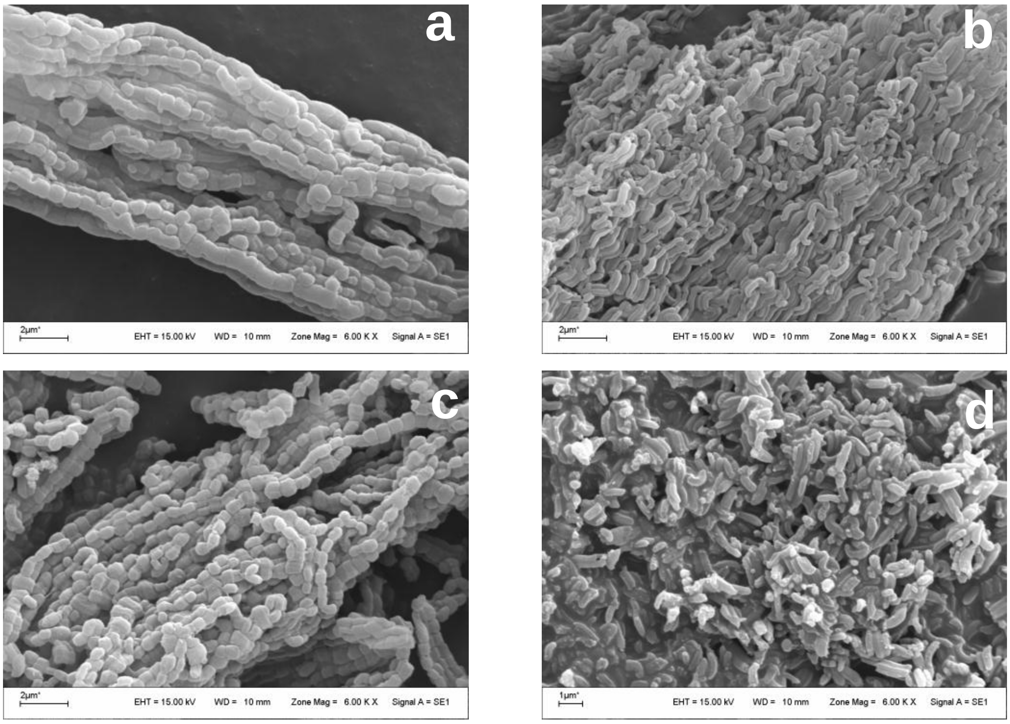
a
2µm*
EHT = 15.00 kV
WD = 10 mm
Zone Mag = 6.00 K X
Signal A = SE1
b
2µm*
EHT = 15.00 kV
WD = 10 mm
Zone Mag = 6.00 K X
Signal A = SE1
c
2µm*
EHT = 15.00 kV
WD = 10 mm
Zone Mag = 6.00 K X
Signal A = SE1
d
1µm*
EHT = 15.00 kV
WD = 10 mm
Zone Mag = 6.00 K X
Signal A = SE1

Figure 5

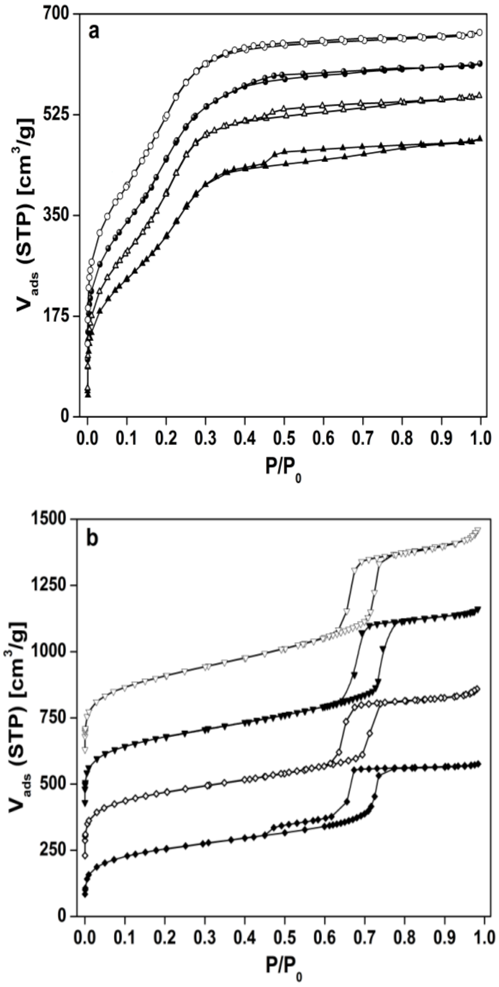

a
700
525
350
175
0
V_{ads} (STP) [cm^3/g]
0.0 0.1 0.2 0.3 0.4 0.5 0.6 0.7 0.8 0.9 1.0
P/P_0
b
1500
1250
1000
750
500
250
0
V_{ads} (STP) [cm^3/g]
0.0 0.1 0.2 0.3 0.4 0.5 0.6 0.7 0.8 0.9 1.0
P/P_0

Figure 6

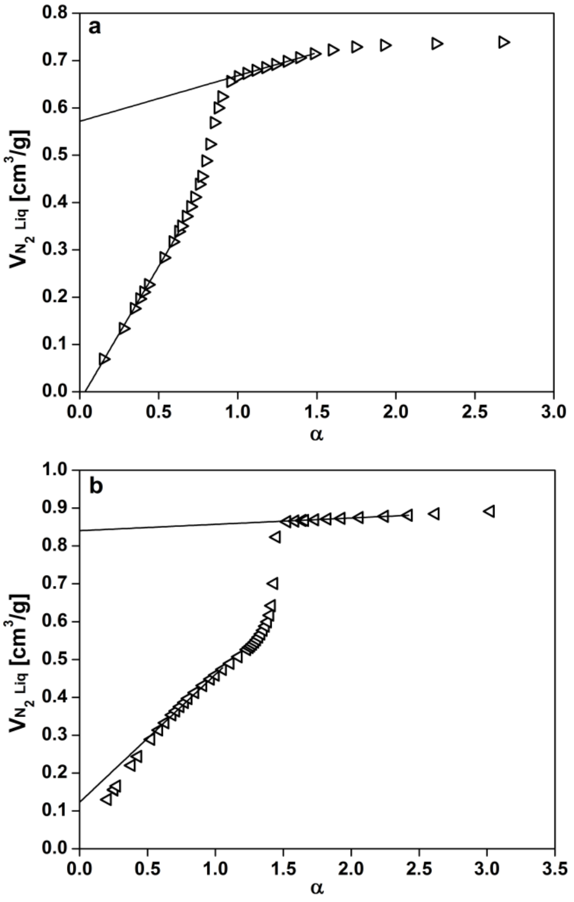
a
$V_{N_2\ Liq}$ [cm^3/g]
0.0
0.1
0.2
0.3
0.4
0.5
0.6
0.7
0.8
0.0
0.5
1.0
1.5
2.0
2.5
3.0
α
b
$V_{N_2\ Liq}$ [cm^3/g]
0.0
0.1
0.2
0.3
0.4
0.5
0.6
0.7
0.8
0.9
1.0
0.0
0.5
1.0
1.5
2.0
2.5
3.0
3.5
α

Figure 7

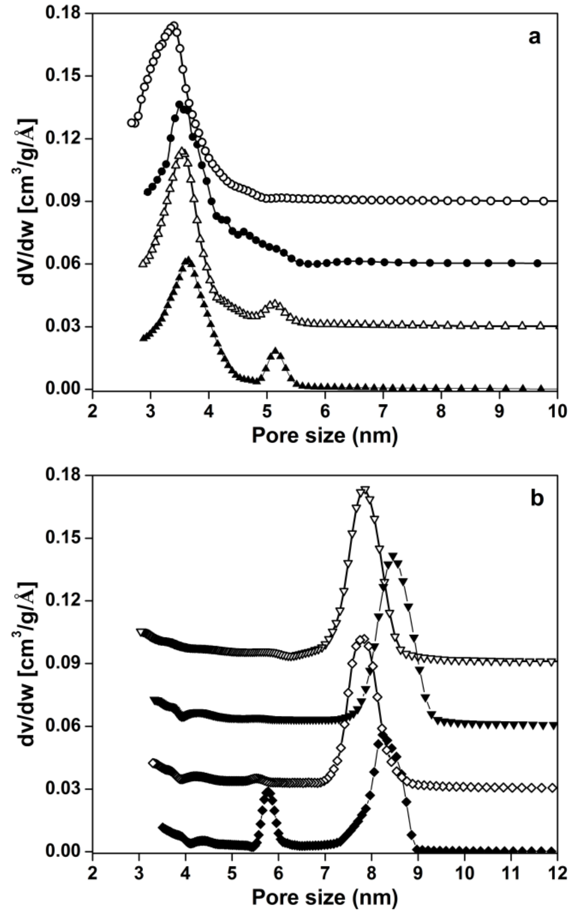
a
dV/dw [cm3/g/Å]
0.00
0.03
0.06
0.09
0.12
0.15
0.18
2
3
4
5
6
7
8
9
10
Pore size (nm)
b
dv/dw [cm3/g/Å]
0.00
0.03
0.06
0.09
0.12
0.15
0.18
2
3
4
5
6
7
8
9
10
11
12
Pore size (nm)

Figure 8

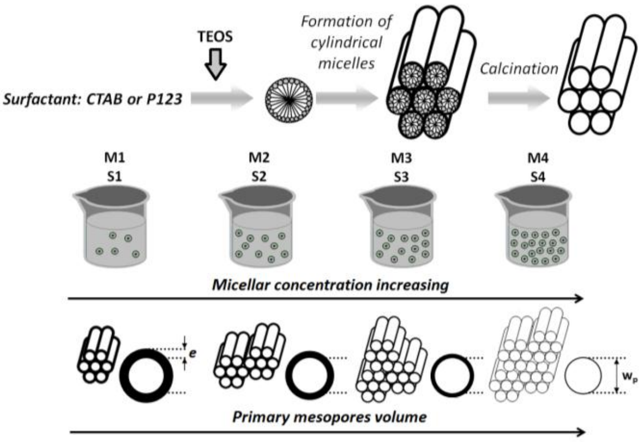
TEOS
Surfactant: CTAB or P123
Formation of cylindrical micelles
Calcination
M1
S1
M2
S2
M3
S3
M4
S4
Micellar concentration increasing
e
w_p
Primary mesopores volume

Table 1

OMM	**Sample**	**Molar ratio**
		CTAB/TEOS
MCM-41	*M1*	0.07
	M2	0.12
	M3	0.17
	M4	0.27
		P123/TEOS
SBA-15	*S1*	0.009
	S2	0.013
	S3	0.017
	S4	0.021

Table 2

		α_s-plot				
Samples	S_{BET} [m^2/g]	$V_{\mu P}$ [cm^3/g]	V_{PMP} [cm^3/g]	S_{ext} [m^2/g]	V_{SMP} [cm^3/g]	V_{TP} [cm^3/g]
M1	1075	0	0.57	180	0.18	0.75
M2	1290	0	0.71	160	0.15	0.86
M3	1340	0	0.76	130	0.11	0.87
M4	1450	0	0.85	60	0.07	0.92
S1	925	0.12	0.72 (0.07) [a]	30	0.05	0.89
S2	975	0.11	0.76	100	0.15	1.02
S3	1005	0.08	0.96	90	0.13	1.17
S4	1110	0.05	1.01	170	0.26	1.32

[a] blocked mesopore volume

Table 3

					VBS method		**NLDFT**
Sample	d_{100} **[nm]**	$w_{p\text{-}XRD}$ **[nm]**	a **[nm]**	e **[nm]**	f_c **[nm]**	w_p **[nm]**	w_p **[nm]**
M1	3.3	3.0	3.8	0.82	0.56	3.6	3.2
M2	3.1	3.0	3.6	0.65	0.56	3.5	3.2
M3	2.9	2.8	3.4	0.58	0.62	3.5	3.2
M4	2.8	2.8	3.3	0.50	0.50	3.4	3.2
S1	10.6 (5.3)*	9.5	12.2	2.7	0.88	8.2	8.1
S2	9.6 (4.8)*	8.8	11.1	2.3	0.78	7.8	7.6
S3	9.5 (4.8)*	9.3	11.0	1.8	0.79	8.5	8.5
S4	9.4 (4.7)*	9.3	10.8	1.6	0.64	7.9	8.1

* correspond to d_{200}